COMMUNICATION

Check for updates

Bionic nanomedicines for microwave-triggered cuproptosis to enhance cancer immunotherapy

Meng Suo,†[a] Ziqi Wang,†[b] Shiwei Zhang,[c] Wei Tang,[a] Dongyan Liang,[a] Xiaoyuan Chen [ID] *[defghijk] and Shipeng Ning [ID] *[a]

Cuproptosis relies on intracellular copper accumulation and shows great potential in tumor therapy. However, the high content of glutathione (GSH) in tumor cells limits its effectiveness. Furthermore, the mechanism of immune activation mediated by cuproptosis remains unclear. To address this, we developed a cancer cell membrane-coated Cu_2O nanoparticle (TC) to induce cuproptosis in tumor cells. After entering tumor cells *via* homologous targeting, the TC released Cu^{2+} in the acidic microenvironment. Cu^{2+} are subsequently reduced to Cu^+ generating hydroxyl radicals through the Fenton reaction. These results led to the downregulation of GSH and eventually sensitized cuproptosis. Microwave (MW)-induced hyperthermia further amplifies these effects. Experimental results demonstrate that TC + MW effectively induces 4T1 cancer cells' cuproptosis both *in vitro* and *in vivo*, significantly inhibiting 4T1 tumor growth with minimal systemic toxicity. The treatment also triggered tumor immunogenic cell death and sensitized T-cell-mediated anti-tumor immunity. TC offers a promising strategy for effective cancer cuproptosis and immunotherapy.

New concepts

In this work, we developed a cancer cell membrane-coated Cu_2O nanoparticle (TC) to induce cuproptosis in tumor cells. After entering tumor cells *via* homologous targeting, the TC released Cu^{2+} in the acidic microenvironment. Cu^{2+} are subsequently reduced to Cu^+ generating hydroxyl radicals through the Fenton reaction. These results led to the downregulation of GSH and eventually sensitized cuproptosis. Microwave-induced hyperthermia further amplifies these effects. Experimental results demonstrate that TC effectively induces 4T1 cancer cells' cuproptosis both *in vitro* and *in vivo*, significantly inhibiting 4T1 tumor growth with minimal systemic toxicity. The treatment of TC also triggered tumor immunogenic cell death and sensitized T-cell-mediated anti-tumor immunity. TC offers a promising strategy for effective cancer cuproptosis and immunotherapy.

1. Introduction

Cuproptosis is a novel mechanism of cell death, and has recently been drawing significant attention in the tumor therapy field.[1–5] Unlike those early-documented cell death mechanisms, cuproptosis primarily relies on the accumulation of intracellular copper ions. Excess copper ions will then bind to acylated proteins involved in the tricarboxylic acid (TCA) cycle, resulting in abnormal aggregation of these proteins and leading to the loss of iron–sulfur cluster proteins.[6] This will inevitably induce proteotoxic stress and result in cell death. Notably, many tumor cells exhibit elevated acylation levels of TCA cycle enzymes, which in particularly are the pyruvate dehydrogenase complex (PDH), and show a greater dependence on mitochondrial metabolism rather than glycolysis.[7] This unique form of cell death offers a promising approach to overcoming resistance to chemotherapy and radiotherapy. Cuproptosis is a copper-dependent form of immunogenic cell death (ICD), involving an immune response through the release

[a] *Research Center of Nanomedicine Technology, The Second Affiliated Hospital of Guangxi Medical University, Nanning, 530000, China. E-mail: nspdoctor@sr.gxmu.edu.cn*

[b] *Department of Oncology, Tongji Hospital, Tongji Medical College, Huazhong University of Science and Technology, Wuhan 430030, China*

[c] *College of Pharmaceutical Sciences, Zhejiang University, Hangzhou, 310058, China*

[d] *Department of Diagnostic Radiology, Yong Loo Lin School of Medicine, National University of Singapore, 119074, Singapore. E-mail: chen.shawn@nus.edu.sg*

[e] *Department of Chemical and Biomolecular Engineering, College of Design and Engineering, National University of Singapore, 117575, Singapore*

[f] *Department of Biomedical Engineering, College of Design and Engineering, National University of Singapore, 117575, Singapore*

[g] *Department of Pharmacy and Pharmaceutical Sciences, Faculty of Science, National University of Singapore, 117544, Singapore*

[h] *Clinical Imaging Research Centre, Centre for Translational Medicine, Yong Loo Lin School of Medicine, National University of Singapore, 117599, Singapore*

[i] *Nanomedicine Translational Research Program, Yong Loo Lin School of Medicine, National University of Singapore, 117597, Singapore*

[j] *Theranostics Center of Excellence (TCE), Yong Loo Lin School of Medicine, National University of Singapore, 138667, Singapore*

[k] *Institute of Molecular and Cell Biology, Agency for Science, Technology, and Research (A*STAR), 138673, Singapore*

† Authors contributed equally.

of many damage-associated molecular patterns (DAMPs) and tumor-associated antigens.[8] Therefore, copper death can reverse the immunosuppressive breast tumor microenvironment and further enhance the efficacy of immune checkpoint inhibitor (ICI)-based immunotherapy. However, the high expression of reduced glutathione (GSH) in tumor cells may inhibit cuproptosis.[9-16] Therefore, promoting GSH depletion and inhibiting copper efflux could be potential strategies to enhance cuproptosis in cancer cells.

Elesclomol has been reported to be an effective copper carrier that has potential in promoting cuproptosis.[5] However, its clinical application is limited by toxic side effects due to the toxic nature of chemo-drugs.[17] In recent years, nanomedicines have attracted considerable attention in cancer therapy due to their multifunctional properties.[18-30] Among these, copper-based nanomaterials have been explored for their Fenton-like activity. Notably, several studies have also used copper-based nanomedicines to trigger cuproptosis.[4,8,31-39] These studies potentially utilize copper-catalyzed Fenton-like reactions to generate ROS and further reduce intracellular GSH levels. However, many of these approaches rely primarily on a single therapeutic modality and lack effective tumor-targeting capability. As a result, high doses of nanoparticles are often required to achieve significant antitumor effects, raising serious concerns regarding systemic toxicity, particularly hepatotoxicity and nephrotoxicity.[40-44] Some non-invasive techniques that can enhance the physicochemical abilities of nanomedicines, such as thermal heating, radiation, or light exposure, can be an alternative solution to address these problems.[43-48] Microwaves offer several advantages including precise and localized heating and can enhance the permeability and cellular uptake of nanoparticles.[49-51] More importantly, microwave-induced mild hyperthermia would then enhance the Fenton-like activity of Cu^+, as proper heating can intensify the efficiency of the Fenton reaction.[52,53] Improving the transport efficiency of nanomedicines into tumors is essential for enhancing therapeutic efficacy and reducing systemic side effects. We believe that modification of microwave irradiation, along with appropriate tumor-targeting modifications, can significantly reduce the required drug dosage and thereby provide a safer and more effective therapeutic strategy.

In this study, a cancer cell membrane-coated Cu_2O nanoparticle (TC) was designed to induce cuproptosis and enhance tumor immunotherapy (Scheme 1). First, cancer cell membrane vesicles (TM) were prepared using a physical extrusion method. TM endow TC with the prolonged blood circulation and enhanced tumor targeting capability. Previous studies have shown that tumor cell membranes can target the same type of tumor cells and tissues through homology.[54,55] After entering the cells, TC would release encapsulated Cu_2O nanoparticles. These nanoparticles would then react with H^+ to produce Cu^{2+}. Cu^{2+} are subsequently reduced to Cu^+ by GSH and generate hydroxyl radicals through the Fenton reaction, which, on the one hand, enhances the cellular oxidative stress and, on the other hand, depletes intracellular GSH. Moreover, this Fenton-like effect can be further enhanced by the introduction of microwave-induced hyperthermia. Finally, the accumulated Cu^+ triggers cuproptosis in tumor cells, which, combined with the enhanced cellular oxidative stress, leads to significant tumor destruction. Experimental results demonstrate that TC effectively induces 4T1 cancer
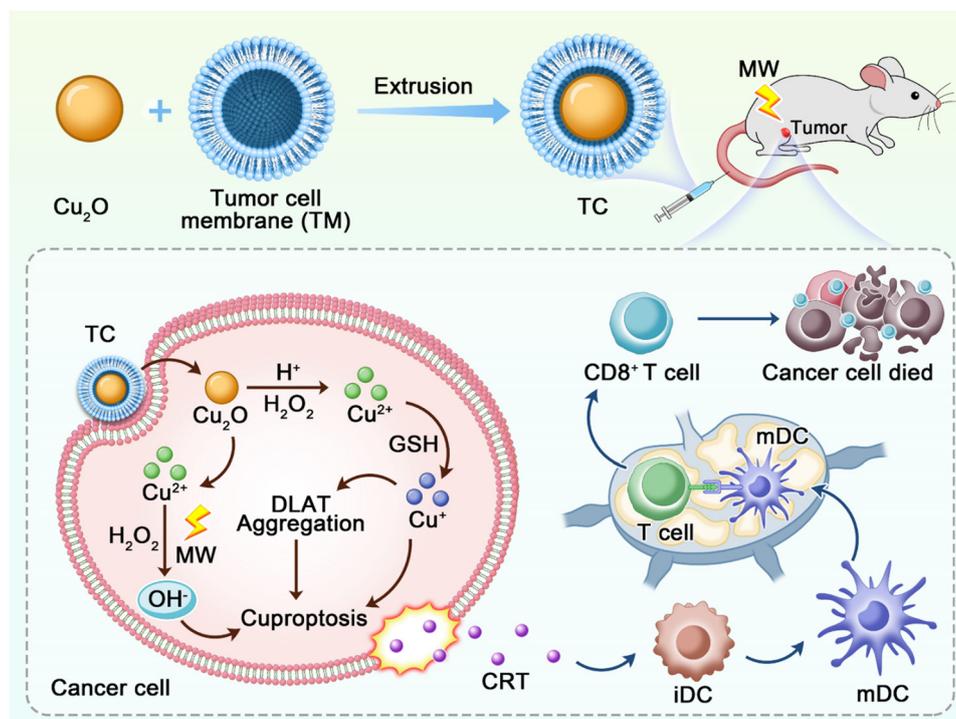
Scheme 1 Schematic illustration of bionic nanomedicines for microwave-triggered cuproptosis to enhance cancer immunotherapy.
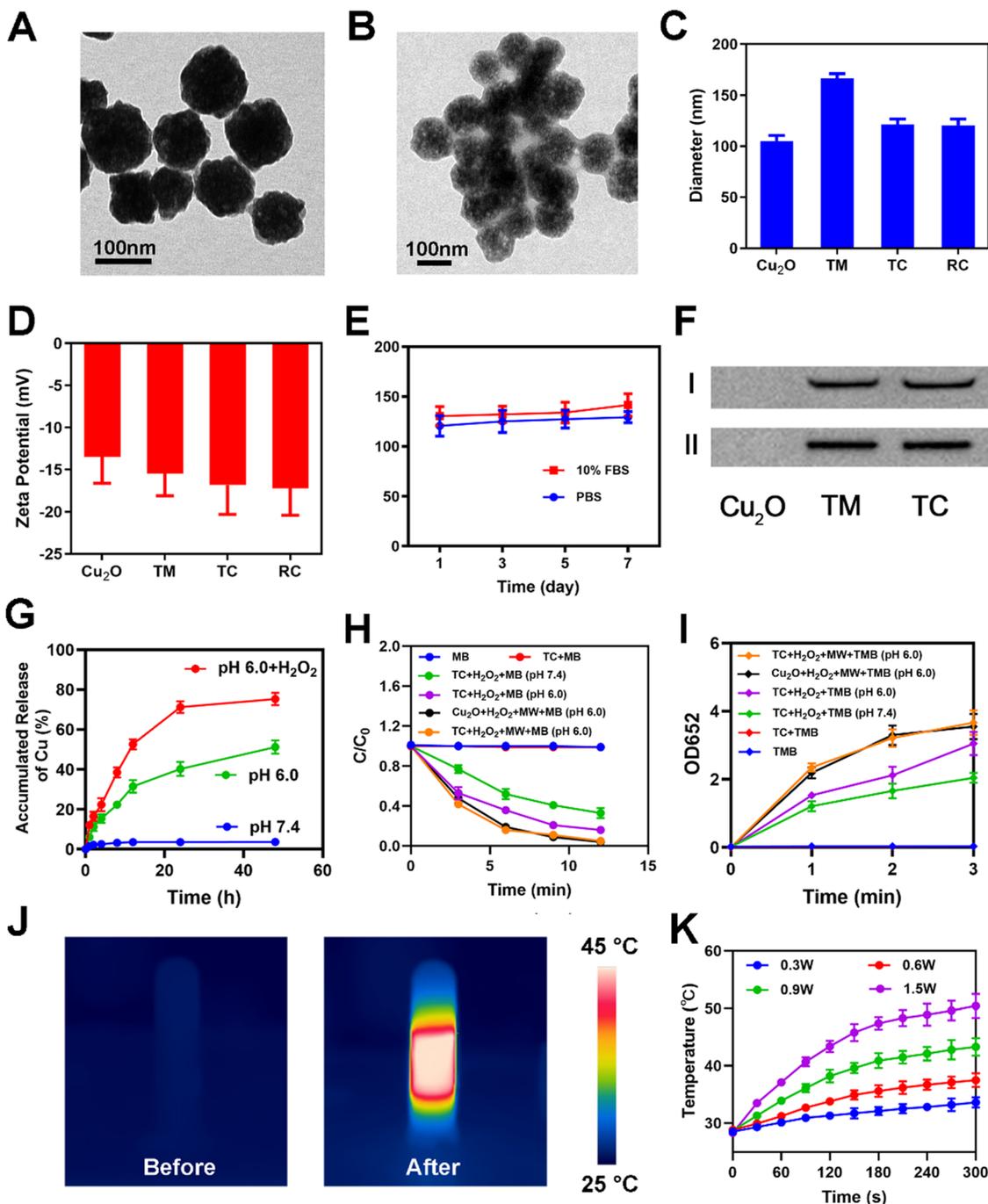
Fig. 1 (A) TEM images of as-prepared Cu_2O and (B) TC. (C) The size and (D) zeta potential of Cu_2O, TM and TC. (E) The hydrodynamic diameter change of TC for 7 days in PBS or 10% FBS solution. (F) Tumor membrane vesicle (TM) marker demonstration, including Na-K ATPase (II) and N-cadherin (I). (G) Accumulated release curves of Cu under different conditions. (H) MB concentration changes *versus* the time under different conditions. (I) The OD value of 652 wavelength change under different conditions, showing the concentration changes of ox-TMB. (J) The temperature changes of Cu_2O solution before and after microwave treatment. (K) Temperature changes of Cu_2O solution over time for different microwave powers. Data are represented as mean $\pm$ SD, $n = 3$.

cells' cuproptosis both *in vitro* and *in vivo*, significantly inhibiting 4T1 tumor growth with minimal systemic toxicity. The treatment of TC also triggered tumor immunogenic cell death and sensitized T-cell-mediated anti-tumor immunity. To the best of our knowledge, this study represents the first investigation into the promoting effect of microwaves on tumor cuproptosis, providing a novel perspective for cancer therapy.

2. Results and discussion

2.1. Synthesis and characterization

The Cu_2O nanoparticles were successfully synthesized firstly, and tumor membrane decoration was conducted used a physical extrusion method afterwards. The TEM images of the as-prepared Cu_2O nanoparticles and TC are shown in Fig. 1A and B.

The Cu_2O nanoparticles exhibit an octahedral structure with a size of approximately 80 nm. After membrane coating, the surface details of the gray cell membrane can be observed. Dynamic light scattering (DLS) experiments were performed to measure the particle sizes of Cu_2O nanoparticles and TC. The results revealed that after coating with the cancer cell membrane, the hydrodynamic diameter increased by about 20 nm (Fig. 1C), and the zeta potential decreased (Fig. 1D). The Cu_2O nanoparticles encapsulated by red blood cell membranes were prepared by a similar method, and the electron microscopy image is shown in Fig. S1. The decrease indicates that the membrane coating can enhance the compatibility of

Cu_2O in the biological environment, which means improved cellular mobility so that they can reach tumor cells more easily. Furthermore, the size of both Cu_2O nanoparticles and TC remained stable in fetal bovine serum (FBS) for one week with no significant changes (Fig. 1E). To further confirm the successful membrane coating, we conducted western blot (WB) analysis to examine the protein on the TC surface. As shown in Fig. 1F, the protein of TC was consistent with that of the tumor vesicles (TM), while Cu_2O nanoparticles did not show this phenomenon. Together, these results would confirm the successful preparation of Cu_2O nanoparticles coated with cancer cell membranes.
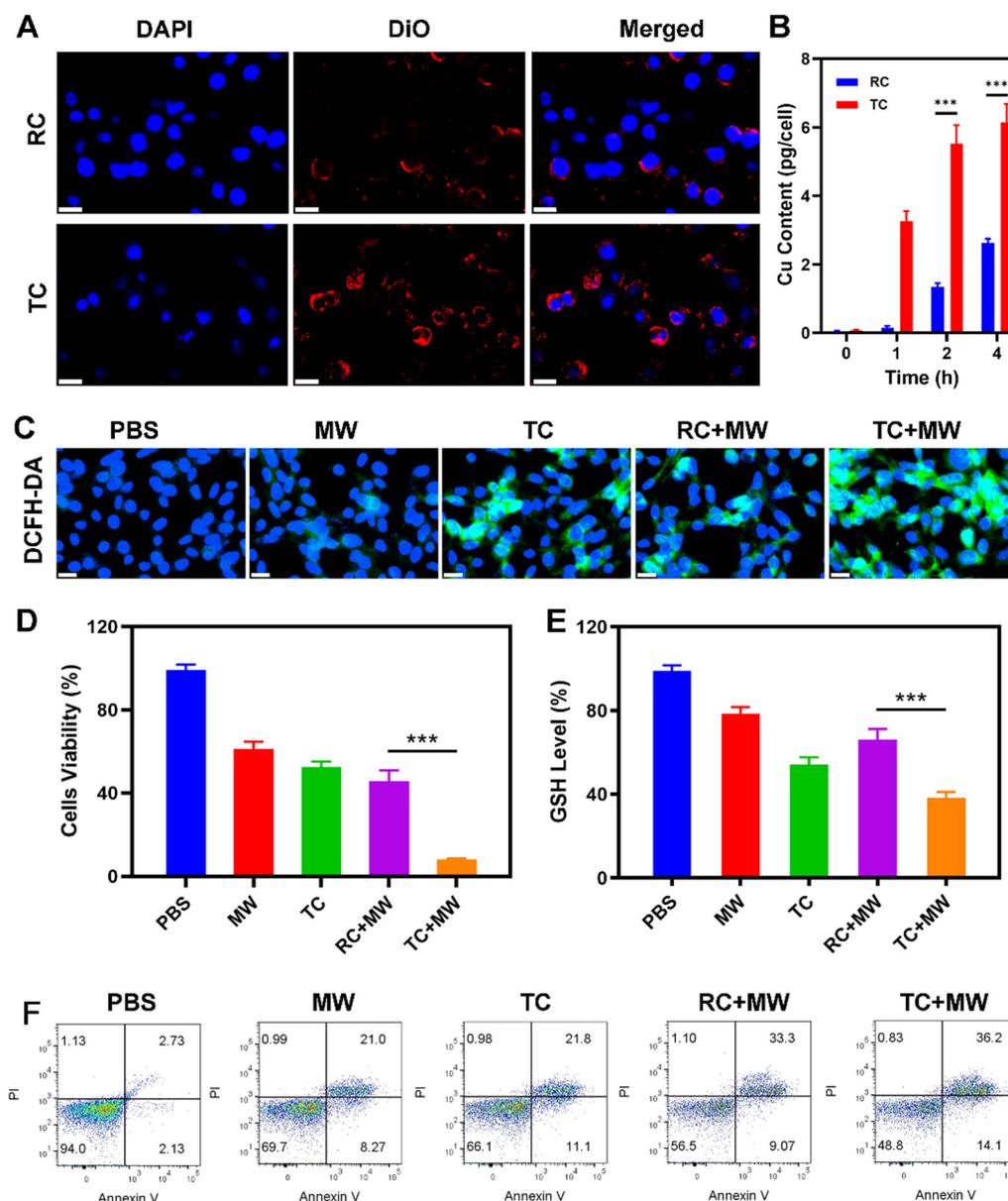
Fig. 2 (A) CLSM images of 4T1 cancer cells incubated with RC and TC for 2 h. Blue: DAPI; red: DiO. (B) Fluorescence intensity of Dio in A. (C) ROS fluorescence images of cancer cells after the indicated treatment. Scale bars: 15 μm. (D) Cell viability after the indicated treatment. (E) GSH level in the cancer cells after the indicated treatment. (F) Cellular apoptosis analysis after treating with different formulations. Data are represented as mean ± SD, n = 3. For variance analysis, one-way analysis of variance (ANOVA) with Tukey's *post hoc* test was used. ***$p < 0.001$.

In the presence of H_2O_2, Cu_2O can rapidly react with H_2O_2 and hydrogen ions (H^+), releasing Cu^{2+}. The reaction can be described using the equation: $Cu_2O + 4H^+ + H_2O_2 \rightarrow 2Cu^{2+} + 3H_2O$. This effect can be confirmed by the results in Fig. 1G. We then used methyl blue (MB) and 3,3',5,5'-tetramethylbenzidine (TMB) as indicators to evaluate the ability of TC to generate hydroxyl radicals ($^{\bullet}OH$) under different conditions. The results in Fig. 1H and I demonstrate that in the presence of H_2O_2, TC not only reduced the MB concentration but also induced color changes in the TMB-containing solution. Electron spin resonance spectroscopy also confirmed the generation of hydroxyl radicals (Fig. S2). Additionally, the rate of hydroxyl radical production was significantly enhanced under acidic conditions and upon microwave treatment, ensuring its efficacy in subsequent therapeutic applications. Furthermore, we validated the heat generation ability of TC upon microwave treatment, illustrating the microwave effect. As shown in Fig. 1J, the solution containing TC exhibited a significant temperature increase after microwave exposure. The heating rate increased with higher microwave power, reaching 50 °C within 5 minutes at a power of $1.5~W~s^{-1}$.

2.2. *In vitro* anticancer efficacy of TC

After confirming the successful coating of Cu_2O nanoparticles with cancer cell membranes, we explored the tumor-targeting capability of TC. A control group, RC, was constructed by replacing the platelet membrane in PTC with red blood cell membranes. Both TC and RC were labeled with the 3,3'-dihexyloxacarbocyanine iodide (Dio) dye to observe their interactions with cancer cell membranes. As shown in Fig. 2A, the TC group exhibited prominent Dio fluorescence on the surface of tumor cells, while the Dio fluorescence in the RC group was significantly weaker, indicating that TC has a superior tumor-targeting ability. Next, we used inductively coupled plasma atomic emission spectrometry (ICP-AES) to measure the copper content in tumor cells after treatment with TC and RC. As shown in Fig. 2B, although the copper content increased in both groups within 4 hours, the copper level in the TC group was significantly higher than in the RC group at the same point, further validating the enhanced tumor-targeting capacity of TC. We then investigated the impact of TC on tumor cells after internalization and *in vitro* antitumor efficacy. As shown in Fig. 2C, the MW group did not produce significant ROS
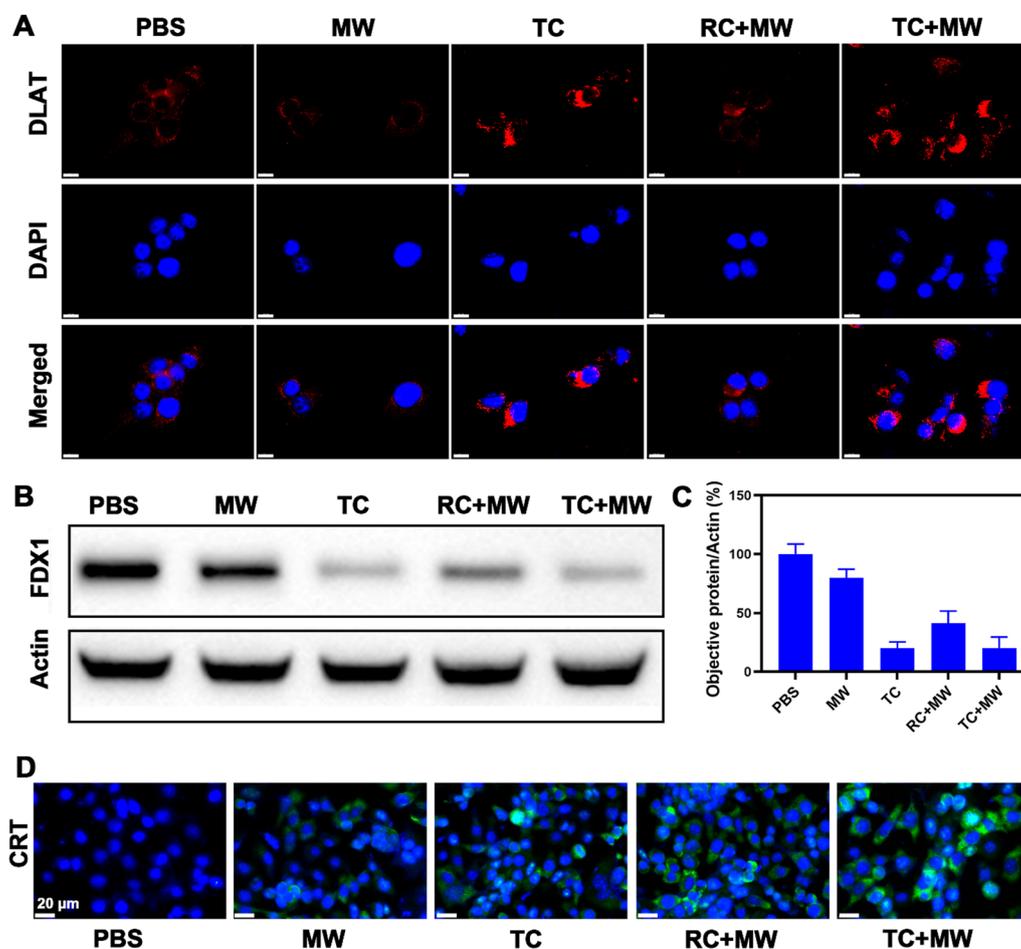

Fig. 3 (A) DLAT fluorescence images of 4T1 cancer cells after the indicated treatment. Scale bars: 15 μm. (B) (B) Fe−S cluster protein expression in cancer cells after the indicated treatments. (C) Gray analysis in cancer cells after the indicated treatments. (D) Fluorescence images of calreticulin (CRT) in 4T1 cells treated with indicated formulations. Data are represented as mean ± SD, $n = 3$.
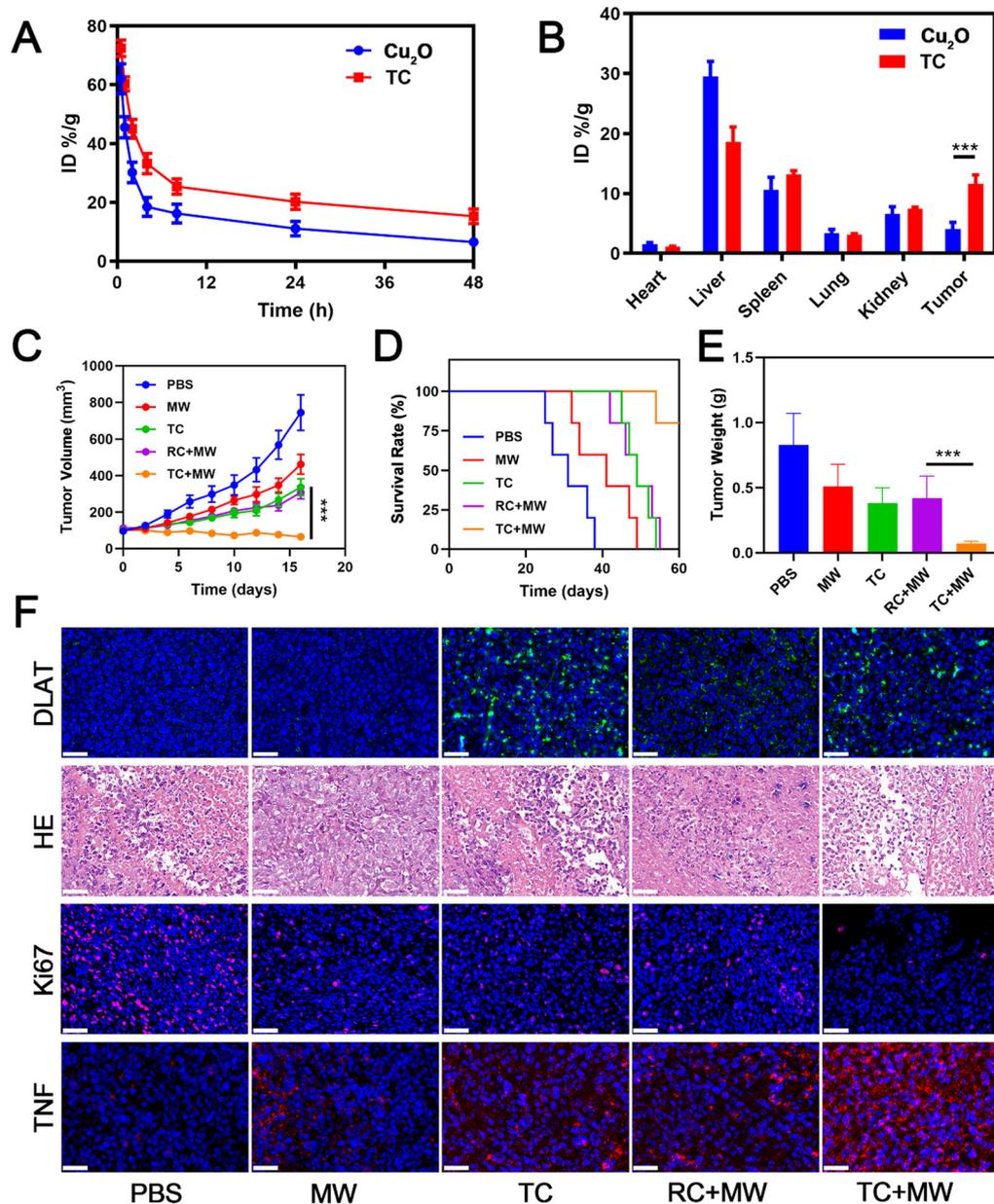
Fig. 4   *In vivo* pharmacokinetic profile of TC and RC in (A) tumors and (B) normal organ. (C) The changes of the tumor volumes of mice after various treatments. (D) The survival probability of mice for various treatments. (E) The changes of the tumor weight of mice after various treatments. (F) DLAT, HE, Ki67 and TNF staining analyses of tumor tissues treated with various treatments. Scale bars: 40 μm. Data are represented as mean ± SD, $n = 5$. For variance analysis, One-way analysis of variance (ANOVA) with Tukey's *post hoc* test was used. ***$p < 0.001$.

compared to the PBS control, suggesting that microwaves (MW) alone did not markedly affect the oxidative environment of the cells. In contrast, TC was able to generate a certain level of ROS upon entering tumor cells, and this effect was significantly enhanced under microwave intervention. To further validate the cytotoxicity of the treatments, we conducted MTT assays, as shown in Fig. 2D. The results demonstrated a trend in cancer cell killing like the ROS production data, with the TC + MW group exhibiting the most potent cytotoxic effect. Additionally, the combined treatment of TC and MW led to substantial depletion of intracellular GSH (Fig. 2E), likely due to the large production of •OH, which significantly consumed GSH. The

results of flow cytometry apoptosis detection showed that the TC + MW group caused the most apoptosis (Fig. 2F). Overall, TC achieves significant tumor cell killing through its efficient ROS generation and GSH depletion capabilities.

2.3.   Induction of cuproptosis in tumor cells by TC *in vitro*

After the investigation of the stress response and cytotoxic effects of TC on tumor cells, we hypothesized that the observed cell death was mediated by the mechanism of cuproptosis. To further investigate this, we evaluated the impact of TC on cuproptosis induction in tumor cells *in vitro*. Fig. 3A–C shows the expression levels of key biomarkers involved in cuproptosis,

including dihydrolipoamide S-acetyltransferase (DLAT) and ferredoxin 1 (FDX1) proteins, under different treatment conditions. Copper ions will bind to acylated components in the tricarboxylic acid (TCA) cycle, leading to the aggregation of acylated proteins and the loss of iron–sulfur cluster proteins during cuproptosis.[8] Both the TC and RC + MW groups showed varying degrees of DLAT aggregation, with the TC + MW group displaying the most prominent aggregation. Additionally, western blot analysis of the FDX1 protein revealed a significant decrease in the FDX1 expression in the TC + MW group, indicating a marked reduction in iron–sulfur cluster proteins. These findings suggest that treatment with PTC + L effectively induces cuproptosis in tumor cells by promoting copper ion accumulation, resulting in the aggregation of acylated proteins and the depletion of essential iron–sulfur cluster proteins, key signatures of this novel cell death pathway. Furthermore, the combination of TC and MW significantly upregulated the expression of calreticulin (Fig. 3D) and facilitated the release of HMGB1 and ATP (Fig. S3), suggesting that it can induce immunogenic cell death (ICD) in 4T1 cells. The occurrence of ICD is crucial for activating T-cell immunity.[10,11,56–60]

Therefore, TC + MW is expected to effectively activate anti-tumor immunity.

2.4. *In vivo* anti-tumor ability of TC

After evaluating the cytotoxic effects and underlying mechanisms of TC on cancer cells, we next explored the *in vivo* antitumor activity. Before this, we should first examine the tumor-targeting capability of TC *in vivo*. As shown in Fig. 4A, compared to naked Cu_2O nanoparticles and RC, TC exhibited superior long-lasting blood circulation. This is primarily attributed to the presence of the cancer cell membrane, which prevents TC from being recognized by the immune system, thereby avoiding phagocytosis and clearance. Moreover, following intravenous injections of TC and RC, we measured the nanoparticle content in tumor tissues and other organs. As shown in Fig. 4B, the copper content in the tumor tissues of the TC group was higher than that in the RC group, further confirming the excellent tumor-targeting ability of TC. Next, we assessed the *in vivo* antitumor efficacy of PTC (Fig. 4C–E). The TC and RC + MW groups showed partial tumor inhibition, while the TC + MW group exhibited significant tumor growth
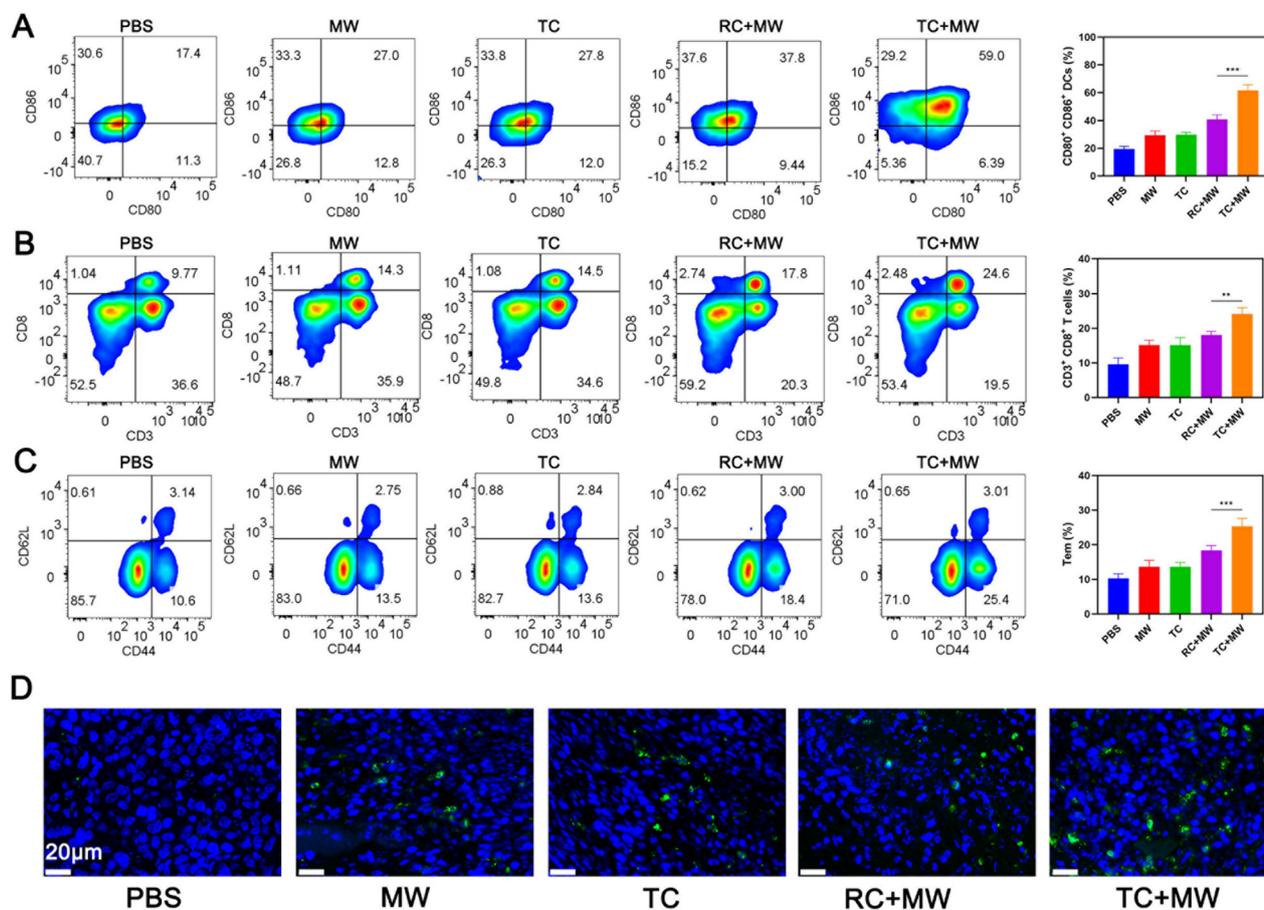

Fig. 5 (A) Representative flow cytometry plots and quantitative analysis of $CD80^+CD86^+$ DC cells in lymph nodes. (B) Representative flow cytometry plots and quantitative analysis of $CD3^+CD8^+$ T cells in tumors. (C) Representative flow cytometry plots and quantitative analysis of $CD44^+CD62L^-$ Tem cells in blood. (D) Immunofluorescence staining of $CD8^+$ T cells (green) in tumors. Data are represented as mean ± SD, $n = 5$. For variance analysis, one-way analysis of variance (ANOVA) with Tukey's *post hoc* test was used. $**p < 0.01$, $***p < 0.001$.

suppression, with the tumor volume reduced by approximately 90%. Furthermore, fluorescence imaging of DLAT in tumor tissues revealed prominent DLAT fluorescence in both the TC and TC + MW groups, indicating that TC effectively induces cuproptosis in tumor cells. Finally, TUNEL, Ki-67, and TNF immunofluorescence staining of tumor tissue sections demonstrated that the TC + MW group induced the most tumor necrosis and growth inhibition (Fig. 4F). To explore the potential immunotherapy mechanism of TC, the activation of the immune response in the mice after different treatments was analyzed. Firstly, the axillary lymph nodes of mice after treatment were digested into single-cell suspensions for flow cytometry analysis to evaluate the maturation of DCs. As shown in Fig. 5A, compared with PBS (17.4%), MW (27.0%), TC (27.8%), and RC + MW (37.8%) treatments, the TC + MW group significantly increased the expression proportion of $CD80^+CD86^+$ DCs (59.0%). The presentation of antigens from

matured DCs to T cells is crucial for activating adaptive immune responses, including the activation of $CD8^+$ T cells and $CD4^+$ T cells that are necessary for inducing anti-tumor immune responses. Likewise, as shown in Fig. 5B, the proportion of antigen-specific T lymphocytes in tumors of mice was investigated by flow cytometry. As a result, the proportion of $CD3^+CD8^+$ T cells in mice treated with TPC was the highest (24.6%). Furthermore, the proportion of effector memory T cells (Tem) was the highest in the TC + MW group (Fig. 5C), indicating that TC + MW treatment activated the long-term anti-tumor immune ability of mice. We performed $CD8^+$ T cell immunofluorescence staining on the tumor tissues of mice after different treatments to examine the T lymphocyte infiltration in tumors, and the results confirmed that the TC + MW treatment group exhibited the highest expression of $CD8^+$ T cells, indicating that TC treatment induced more infiltration of T cells (Fig. 5D). In addition, we established a bilateral tumor
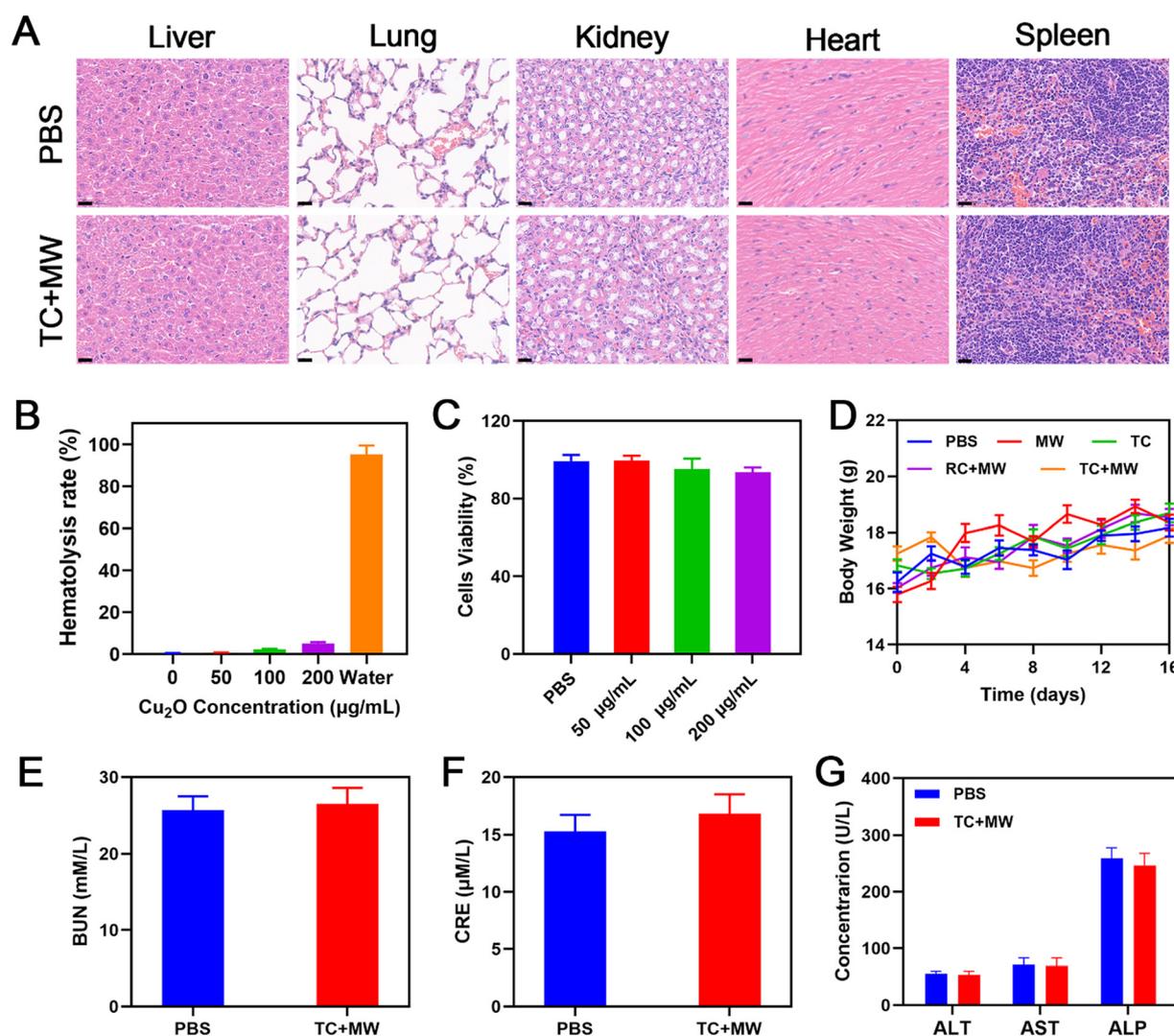

Fig. 6 (A) H&E staining of the normal tissues (scale bars: 200 μm). (B) Blood test results of mice under different Cu_2O treatments. (C) Cell viability under different Cu_2O treatments. (D) The changes of the body weight of mice after various treatments. Blood biochemical analysis of mice 18 days after different treatments, and (E and F) kidney and (G) liver toxicity test results. Data are represented as mean ± SD, n = 5.

model, as shown in Fig. S4. TC + MW treatment of the primary tumor could significantly inhibit the growth of the distal tumor, which also indicates that it can enhance the anti-tumor immune function of the body.

2.5. *In vivo* toxicity study

In biomedical applications, the potential *in vivo* toxicity of nano-materials is always a crucial consideration. Therefore, in this study, we conducted a series of safety assessments to evaluate the feasibility of our proposed therapeutic approach. Firstly, no significant signs of organ damage were observed in H&E-stained tissue sections (Fig. 6A). Hemolysis tests also showed that, despite the concentration of TC (calculated based on Cu_2O) reaching 200 μg mL^{-1}, its concentration in the blood remained relatively low (Fig. 6B). Even at a relatively high concentration of cuprous oxide, no high normal cytotoxicity was observed (Fig. 6C). Throughout the entire vivo treatment period, no significant changes in the body weight were observed in mice (Fig. 6D). Moreover, renal function markers, including creatinine (CRE) and blood urea nitrogen (BUN), remained within normal ranges (Fig. 6E and F), as did liver function markers such as alanine aminotransferase (ALT), aspartate aminotransferase (AST), and alkaline phosphatase (ALP) (Fig. 6G). These results suggest that TC exhibits excellent biocompatibility.

3. Conclusions

In summary, we have developed a TC system to induce cuproptosis in tumor cells. TC effectively targets tumor tissues and rapidly releases copper ions within cancer cells. Additionally, under microwave intervention, TC can produce a large amount of hydroxyl radicals upon entering the cells, leading to the depletion of intracellular glutathione (GSH). Furthermore, the copper ions released by TC significantly increase the occurrence of cuproptosis in tumor cells. Our experiments have demonstrated the cytotoxic effects of TC on cancer cells both *in vitro* and *in vivo*. In the future, this strategy to enhance cuproptosis holds potential for improving the sensitivity of traditional cancer therapies and may provide new insights for the design of copper death-based nanomedicines.

Conflicts of interest

X. C. is a co-founder of and holds shares in Yantai Lannacheng Biotechnology Co., Ltd.

Data availability

The data supporting this article have been included as part of the SI. See DOI: **https://doi.org/10.1039/d5nh00425j**.

Acknowledgements

References

1 D. Tang, X. Chen and G. Kroemer, *Cell Res.*, 2022, **32**, 417–418.

2 Y. Wang, L. Zhang and F. Zhou, *Cell. Mol. Immunol.*, 2022, **19**, 867–868.

3 W. Xu, J. Qian, G. Hou, T. Wang, J. Wang, Y. Wang, L. Yang, X. Cui and A. Suo, *Adv. Funct. Mater.*, 2022, **32**, 2205013.

4 S. Ning, M. Lyu, D. Zhu, J. W. Y. Lam, Q. Huang, T. Zhang and B. Z. Tang, *ACS Nano*, 2023, **17**, 10206–10217.

5 P. Tsvetkov, S. Coy, B. Petrova, M. Dreishpoon, A. Verma, M. Abdusamad, J. Rossen, L. Joesch-Cohen, R. Humeidi, R. D. Spangler, J. K. Eaton, E. Frenkel, M. Kocak, S. M. Corsello, S. Lutsenko, N. Kanarek, S. Santagata and T. R. Golub, *Science*, 2022, **375**, 1254–1261.

6 P. Tsvetkov, S. Coy, B. Petrova, M. Dreishpoon, A. Verma, M. Abdusamad, J. Rossen, L. Joesch-Cohen, R. Humeidi, R. D. Spangler, J. K. Eaton, E. Frenkel, M. Kocak, S. M. Corsello, S. Lutsenko, N. Kanarek, S. Santagata and T. R. Golub, *Science*, 2022, **375**, 1254–1261.

7 N. M. Anderson, P. Mucka, J. G. Kern and H. Feng, *Protein cell*, 2018, **9**, 216–237.

8 N. Zhang, W. Ping, K. Rao, Z. Zhang, R. Huang, D. Zhu, G. Li and S. Ning, *J. Controlled Release*, 2024, **371**, 204–215.

9 D. Wang, Z. Tian, P. Zhang, L. Zhen, Q. Meng, B. Sun, X. Xu, T. Jia and S. Li, *Biomed. Pharmacother.*, 2023, **163**, 114830.

10 N. Zhang, W. Ping, J. Xiang, S. Chu, D. Li, S. Ning, D. Zhu, W. Zeng and Q. Xu, *Adv. Healthcare Mater.*, 2024, e2401362, DOI: **10.1002/adhm.202401362**.

11 Z. Chen, Z. Liu, Y. Zhou, K. Rao, J. Lin, D. Zhu, S. Ning and H. Wang, *Mater. Today Bio*, 2024, **28**, 101217.

12 , DOI: **10.3390/pharmaceutics16060833**.

13 S. Ning, T. Zhang, M. Lyu, J. W. Y. Lam, D. Zhu, Q. Huang and B. Z. Tang, *Biomaterials*, 2023, **295**, 122034.

14 H. Chen, X. Luo, Q. Huang, Z. Liu, M. Lyu, D. Chen, J. Mo and D. Zhu, *Chem. Eng. J.*, 2023, **476**, 146276.

15 D. Zhu, R. Ling, H. Chen, M. Lyu, H. Qian, K. Wu, G. Li and X. Wang, *Nano Res.*, 2022, **15**, 7320–7328.

16 D. Zhu, T. Zhang, Y. Li, C. Huang, M. Suo, L. Xia, Y. Xu, G. Li and B. Z. Tang, *Biomaterials*, 2022, **283**, 121462.

17 A. Elgogary, Q. Xu, B. Poore, J. Alt, S. C. Zimmermann, L. Zhao, J. Fu, B. Chen, S. Xia, Y. Liu, M. Neisser, C. Nguyen, R. Lee, J. K. Park, J. Reyes, T. Hartung, C. Rojas, R. Rais, T. Tsukamoto, G. L. Semenza, J. Hanes, B. S. Slusher and A. Le, *Proc. Natl. Acad. Sci. U. S. A.*, 2016, **113**, E5328–5336.

18 Y. Guo, S. Ding, C. Shang, C. Zhang, M. Li, Q. Zhang, L. Gu, B. C. Heng, S. Zhang, F. Mei, Y. Huang, X. Zhang, M. Xu, J. Jiang, S. Guo, X. Deng and L. Chen, *Adv. Mater.*, 2023, e2306292, DOI: **10.1002/adma.202306292**.

19 J. Liu, S. Dong, S. Gai, Y. Dong, B. Liu, Z. Zhao, Y. Xie, L. Feng, P. Yang and J. Lin, *ACS Nano*, 2023, **17**, 20402–20423.

20 M. Huo, L. Wang, Y. Wang, Y. Chen and J. Shi, *ACS Nano*, 2019, **13**, 2643–2653.

21 F. Cao, Y. Sang, C. Liu, F. Bai, L. Zheng, J. Ren and X. Qu, *ACS Nano*, 2022, **16**, 855–868.

22 G. Xiong, D. Huang, L. Lu, X. Luo, Y. Wang, S. Liu, M. Chen, S. Yu, M. Kappen, C. You, S. Lu, Y. Yu, J. Lu and F. Lin, *Small Methods*, 2022, **6**, e2200379.

23 J. Qian, A. J. M. Aldai, W. Xu, T. Wang, K. Zhao, Y. Wang, J. Fan and A. Suo, *Carbohydr. Polym.*, 2025, **352**, 123201.

24 F. Hu, J. Huang, T. Bing, W. Mou, D. Li, H. Zhang, Y. Chen, Q. Jin, Y. Yu and Z. Yang, *Adv. Sci.*, 2024, **11**, e2309388.

25 S. Lu, Y. Li and Y. Yu, *Adv. Mater.*, 2024, e2404971, DOI: **10.1002/adma.202404971**.

26 W. Xu, Y. Wang, G. Hou, J. Wang, T. Wang, J. Qian and A. Suo, *Adv. Healthcare Mater.*, 2023, **12**, e2202949.

27 W. Xu, A. Suo, A. J. M. Aldai, Y. Wang, J. Fan, Y. Xia, J. Xu, Z. Chen, H. Zhao, M. Zhang and J. Qian, *ACS Nano*, 2024, **18**, 30053–30068.

28 H. Li, S. Han, C. Dong and Z. Liu, *Oncol. Transl. Med.*, 2025, **11**, 17–28.

29 K. Zheng, R. Song, R. Li, M. Liu, Y. Ba, W. Jiang and K. Fan, *Oncol. Transl. Med.*, 2024, **10**, 151–161.

30 Y. Li, Z. Li, Y. Li, X. Gao, T. Wang, X. Ma and M. Wu, *Oncol. Transl. Med.*, 2024, **10**, 212–222.

31 H. Wu, F. Chen, C. You, Y. Zhang, B. Sun and Q. Zhu, *Small*, 2020, **16**, e2001805.

32 X. Meng, K. Zhou, Y. Qian, H. Liu, X. Wang, Y. Lin, X. Shi, Y. Tian, Y. Lu, Q. Chen, J. Qian and H. Wang, *Small*, 2022, **18**, e2107422.

33 B. Ma, S. Wang, F. Liu, S. Zhang, J. Duan, Z. Li, Y. Kong, Y. Sang, H. Liu, W. Bu and L. Li, *J. Am. Chem. Soc.*, 2019, **141**, 849–857.

34 Y. Zhang, S. Li, X. Fang, B. Miao, Y. Wang, J. Liu, G. Nie and B. Zhang, *Nanophotonics*, 2022, **11**, 5189–5204.

35 W. F. Song, J. Y. Zeng, P. Ji, Z. Y. Han, Y. X. Sun and X. Z. Zhang, *Small*, 2023, **19**, e2301148.

36 Z. Tang, S. Jiang, W. Tang, Q. He, H. Wei, C. Jin, S. Wang and H. Zhang, *Mol. Pharm.*, 2023, **20**, 1717–1728.

37 S. Lu, Y. Li and Y. Yu, *Adv. Mater.*, 2024, **36**, e2404971.

38 H. Chen, X. Luo, W. Cai, S. Wang, J. Xiang, Z. Liu and D. Zhu, *Int. J. Nanomed.*, 2023, **18**, 7533–7541.

39 T. Chen, X. Luo, L. Zhu, J. Xiang, C. Fang, D. Zhu, G. Li and Y. Duo, *Chem. Eng. J.*, 2023, **467**, 143386.

40 J. Xie, L. Gong, S. Zhu, Y. Yong, Z. Gu and Y. Zhao, *Adv. Mater.*, 2019, **31**, e1802244.

41 E. Mirhadi, M. Mashreghi, A. Askarizadeh, A. Mehrabian, S. H. Alavizadeh, L. Arabi, A. Badiee and M. R. Jaafari, *Sci. Rep.*, 2022, **12**, 11310.

42 D. Zhu, M. Lyu, Q. Huang, M. Suo, Y. Liu, W. Jiang, Y. Duo and K. Fan, *ACS Appl. Mater. Interfaces*, 2020, **12**, 36928–36937.

43 C. Huang, F. B. Wang, L. Liu, W. Jiang, W. Liu, W. Ma and H. Zhao, *Adv. Healthcare Mater.*, 2021, **10**, e2002207.

44 D. Zhu, Z. Zheng, G. Luo, M. Suo, X. Li, Y. Duo and B. Z. Tang, *Nano Today*, 2021, **37**, 101091.

45 H. Zhang, J. Li, Y. Chen, J. Wu, K. Wang, L. Chen, Y. Wang, X. Jiang, Y. Liu, Y. Wu, D. Jin and W. Bu, *Adv. Mater.*, 2021, e2100472, DOI: **10.1002/adma.202100472**.

46 N. Tao, L. Jiao, H. Li, L. Deng, W. Wang, S. Zhao, W. Chen, L. Chen, C. Zhu and Y. N. Liu, *ACS Nano*, 2023, **17**, 22844–22858.

47 Y. Pan, M. Suo, Q. Huang, M. Lyu, Y. Jiang, S. Wang, W. Tang, S. Ning and T. Zhang, *Aggregate*, 2024, **5**, e432, DOI: **10.1002/agt2.432**.

48 M. Lyu, M. Luo, J. Li, O. U. Akakuru, X. Fan, Z. Cao, K. Fan and W. Jiang, *Adv. Funct. Mater.*, 2023, **33**, 2306930, DOI: **10.1002/adfm.202306930**.

49 Y. Wang, J. Stang, M. Yu, M. Tsvetkov, C. C. Wu, X. Qin, E. Chung, M. Moghaddam and W. Wu, *Adv. Mater. Technol.*, 2016, **1**(3), 1600038.

50 A. J. Wilson, M. Rahman, P. Kosmas and M. Thanou, *Nanoscale Adv.*, 2021, **3**, 3417–3429.

51 Z. Zeng, X. Sun, Z. Huang, C. Fu, J. Ren, M. Niu, L. Tan, X. Ren, Q. Wu and X. Meng, *Colloids Surf., B*, 2022, **217**, 112616.

52 J. A. Zazo, G. Pliego, S. Blasco, J. A. Casas and J. J. Rodriguez, *Ind. Eng. Chem. Res.*, 2011, **50**, 866–870.

53 N. Nuñez, E. Lima, M. Vásquez Mansilla, G. F. Goya, Á. Gallo-Cordova, M. D. P. Morales and E. L. Winkler, *Appl. Surf. Sci.*, 2024, **656**, 159655.

54 S. Y. Li, H. Cheng, B. R. Xie, W. X. Qiu, J. Y. Zeng, C. X. Li, S. S. Wan, L. Zhang, W. L. Liu and X. Z. Zhang, *ACS Nano*, 2017, **11**, 7006–7018.

55 W. Xie, W. W. Deng, M. Zan, L. Rao, G. T. Yu, D. M. Zhu, W. T. Wu, B. Chen, L. W. Ji, L. Chen, K. Liu, S. S. Guo, H. M. Huang, W. F. Zhang, X. Zhao, Y. Yuan, W. Dong, Z. J. Sun and W. Liu, *ACS Nano*, 2019, **13**, 2849–2857.

56 S. Ning, P. Shangguan, X. Zhu, X. Ou, K. Wang, M. Suo, H. Shen, X. Lu, X. Wei, T. Zhang, X. Chen and B. Z. Tang, *J. Am. Chem. Soc.*, 2025, **147**, 7433–7444.

57 S. Ning, X. Zhang, M. Suo, M. Lyu, Y. Pan, Y. Jiang, H. Yang, J. W. Yip Lam, T. Zhang, L. Pan and B. Z. Tang, *Cell Rep. Phys. Sci.*, 2023, **4**, 101505.

58 M. Suo, H. Shen, M. Lyu, Y. Jiang, X. Liao, W. Tang, Y. Pan, T. Zhang, S. Ning and B. Z. Tang, *Small*, 2024, 2400666, DOI: **10.1002/smll.202400666**.

59 X. Yao, H. Yang, S. Guo, Y. Liu, Q. Zhang, Z. Zhou, M. Li and Z. Luo, *Biomaterials*, 2025, **322**, 123391.

60 M. Li, Y. Li, X. Yao, Y. Liu, K. Cai, H. Yang and Z. Luo, *Biomaterials*, 2025, **317**, 123096.